

Interaction of deuterium with defects in silicon studied by means of channeling

B. Bech Nielsen

Institute of Physics, University of Aarhus, DK-8000 Aarhus C, Denmark

(Received 11 May 1987; revised manuscript received 13 October 1987)

The lattice location of deuterium ion-implanted at low temperatures into silicon has been studied by means of the channeling technique. The channeling analysis is carried out at 30 K along the major axes and planes by means of the $D(^3\text{He},p)^4\text{He}$ nuclear reaction. Irradiation at 30 K with the analyzing beam induces a dramatic annealing of lattice defects, and during this process, deuterium atoms are trapped at defects. After the beam-induced annealing, 80% of the deuterium atoms are located close to bond-center sites, while the remaining 20% are located close to tetrahedral sites. After annealing at ~ 140 K, the fraction of deuterium atoms located close to bond-center sites decreases to 70%, whereas the near-tetrahedral component increases to 30%. The near-tetrahedral component anneals out at ~ 500 K, where all the deuterium atoms are moving to near bond-center sites. The results are discussed together with previous infrared-absorption studies, and a consistent interpretation is presented.

I. INTRODUCTION

The interaction of hydrogen with defects in silicon¹⁻⁹ has been studied intensively during the last decade. In spite of this, there is not much direct information available on the structure of the hydrogen-related defects. Picraux and Vook¹ applied the channeling technique to study the lattice location of deuterium, ion-implanted into silicon at room temperature, and found that deuterium atoms were displaced by 1.6 Å from lattice sites in antibonding directions. On the other hand, infrared-absorption measurements²⁻⁵ showed that hydrogen atoms implanted into silicon form Si—H bonds, in agreement with the generally accepted view that hydrogen is trapped at dangling bonds.^{10,11} As vacancy-type defects are created in great numbers during ion implantation, it may be expected that a substantial part of the hydrogen atoms will saturate the broken bonds and thus be located close to bond centers, ~ 1.47 Å (bond length in silane¹²) away from a silicon atom. Apparently, this is contradicted by the channeling results even though some configurational models have been proposed to explain the infrared and the channeling measurements consistently.^{5,13} The present work is directed towards this problem and reports on the lattice location of implanted deuterium in silicon in the temperature range 30–500 K.

Hydrogen in silicon is currently of great interest due to the promising technological implications, e.g., production of large-area, low-cost solar cells based on amorphous material. Various chemical forms of hydrogen have been applied as a standard routine during semiconductor processing, but its importance was not fully recognized until Spear and Le Comber¹⁴ succeeded in doping hydrogenated amorphous silicon.¹⁵ Since then, it has been demonstrated that hydrogen can passivate almost all types of centers in silicon such as deep levels,¹⁶ point defects,⁸ dislocations,⁶ and grain boundaries.^{9,10} The hydrogen atoms saturate the dangling bonds associated with these centers, and hydrogenation thus passivates potent life-

time killers.

The properties of hydrogen in hyperpure undamaged crystalline silicon are very difficult to determine experimentally due to the strong interaction of hydrogen with impurities and defects and to the very low solubility.¹⁷ Thus the lattice location of atomic hydrogen in the silicon crystal (the solution site) has not yet been determined experimentally. A good "guess" on a solution site may be the *M* site (see Fig. 1) suggested by Corbett *et al.*¹⁸ on the basis of modified neglect of diatomic overlap (MNDO) calculations. However, the position is likely to be dependent on the charge state of the hydrogen,¹⁹ and furthermore the reliability of such a chemical-cluster calculation in a description of solid-state properties may be questioned.

In vacuum, the hydrogen molecule is energetically favored by 2.24 eV/atom (Ref. 12) compared to the atomic state, and it is natural to speculate on the formation of hydrogen molecules inside the silicon lattice. Hydrogen in metals is present in the atomic form due to the effective screening by the free electrons.²⁰ In group-IV semiconductors, the valence electrons form strong covalent bonds, leaving open vacuumlike regions around the tetrahedral sites, where the formation of hydrogen molecules may be expected. This is confirmed by theoretical calculations,^{18,19} but the presence of molecules has not yet been established experimentally.

A controlled method for the introduction of hydrogen into crystalline silicon is ion implantation. Among the advantages of the method is the possibility of introducing hydrogen at any temperature and in concentrations exceeding by far the solubility. Moreover, the introduction of defects in the implantation process makes it ideal in studies of hydrogen-defect interactions.

Previous information on the bonding properties of hydrogen implanted into silicon has primarily been obtained by means of infrared-absorption spectroscopy.^{2-5,21} (For a comprehensive review, see the recent paper by Cardona.²²) After room-temperature implantation, a large

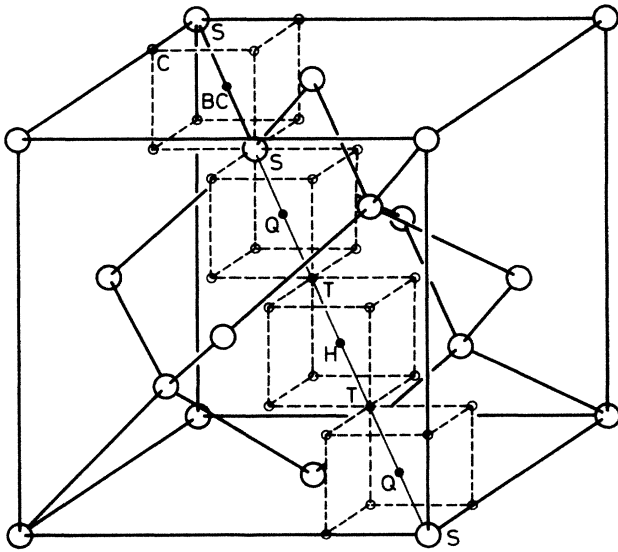


FIG. 1. The conventional unit cell in the silicon lattice, with various impurity sites being indicated, substitutional (*S*), bond-center (*BC*), antibonding (*Q*), tetrahedral (*T*), hexagonal (*H*) and *C* sites (\circ). The *M* sites are located in the middle between two adjacent *C* sites.

number of absorption lines have been observed²⁻⁵ in the frequency range of the stretching-mode vibrations of silane. Recently, Shi *et al.*⁴ and Mukashev *et al.*⁵ suggested structural models for the hydrogen-related defects giving rise to some of these lines. The models of Shi *et al.* were based on quantitative considerations of the effect of the local environment on the Si-H stretch frequency, whereas Mukashev *et al.* based their interpretations on the annealing behavior and dose dependence of the absorption lines. The absorption spectra are less complex after implantation at low temperatures.³ Stein³ observed a major stretch-frequency line at 1990 cm^{-1} and weaker lines at 1840, 1885, and 2060 cm^{-1} after implantation at 80 K. The 1990- cm^{-1} line annealed out around 140–150 K, where the intensities of the 1840- and 2060- cm^{-1} lines increased. The activation energy for the annealing of the 1990- cm^{-1} line was 0.34 eV, and Stein³ ascribed this stage to the migration of monovacancies.

In semiconductors, various techniques such as EPR, photoluminescence, infrared-absorption spectroscopy, and deep-level transient spectroscopy (DLTS) can give information on the symmetry of impurity-related centers. This may be used to model the geometrical structure of the center, but, especially in the cases of low symmetry, the result is often dubious if no further structural information is available. Such information may be obtained by lattice-location experiments, and in the case of hydrogen, where many techniques fail to detect related signals (e.g., no EPR signal²³), the detailed lattice location is of crucial importance for the understanding of the hydrogen-defect interaction.

Besides the channeling experiment of Picraux and Vook,¹ there are a few other localization studies worth mentioning in this context. Sigle *et al.*²⁴ and Maier²⁵ reported on blocking experiments of positive pions (π^+) in

germanium. Their results were interpreted in terms of hexagonal-site occupancy at temperatures below 60 K and tetrahedral-site occupancy above 80 K (see Fig. 1). Furthermore, Patterson *et al.*²⁶ performed blocking-type experiments on positive muons (μ^+) in Czochralski-grown silicon. Patterson²⁷ suggested that the anomalous muon (μ^*) is located close to the antibonding position reported by Picraux and Vook¹ for ion-implanted deuterium. Experiments on float-zone material,²⁷ however, indicated that this interpretation might be wrong.

In the present work, the channeling technique has been applied to determine the lattice location of deuterium ion-implanted into silicon. The objective has been to study the interaction of deuterium with defects and to relate the lattice location to the bonding properties obtained from previous infrared-absorption measurements.^{2,3}

The paper is organized in the following way. After this introduction, the experimental setup is discussed in Sec. II, together with some details of the measurements. Section III summarizes the results of our measurements on the detailed structure and concentration of defects created by the deuterium implantation at 30 K. In Sec. IV is given a brief description of the computer simulations used in the interpretation of the channeling experiments. The results are presented in Sec. V and discussed together with those of other measurements in Sec. VI.

A part of this work has been described in a brief report published previously.²⁸

II. EXPERIMENTAL DETAILS

The experimental setup for the *in situ* deuterium implantation and the subsequent analysis by means of the $\text{D}(^3\text{He}, p)^4\text{He}$ nuclear reaction is shown schematically in Fig. 2. The silicon target was placed in a motor-driven x - y goniometer with an angular resolution of $\sim 0.01^\circ$. The target could be translated perpendicularly to the scattering plane, whereby analysis on several beam spots was possible.

In order to keep the temperature low during implantations, the goniometer head was in thermal contact with a helium-gas cryogenic cooler via a flexible copper braid. High thermal resistance between the goniometer drive and the sample was obtained by a thin (0.15 mm) stainless-steel tube, together with a piece of ceramic glass. In addition, a resistive heater allowed the temperature of the target to be varied continuously between 30 and 500 K. The temperature was measured by a platinum resistance thermometer placed in good thermal contact with the target holder. Finally, the target temperature could, via an electronic feedback circuit, be increased at a constant rate (0.1–10 K/min).

The silicon single crystals with either $\langle 100 \rangle$, $\langle 110 \rangle$, or $\langle 111 \rangle$ orientation were cut from a $\langle 111 \rangle$ rod made of *n*-type, phosphorus-doped, float-zone material with a high resistivity (3–5 $\text{k}\Omega\text{cm}$). The sample sizes were $\sim 8 \times 8 \times 2 \text{ mm}^3$, and the quoted impurity concentrations were $\leq 10^{15} \text{ cm}^{-3}$. Finally, the oxide layer on the surface was always removed with a HF etch just before the sample was inserted into the vacuum chamber.

The target chamber was pumped by a diffusion pump,

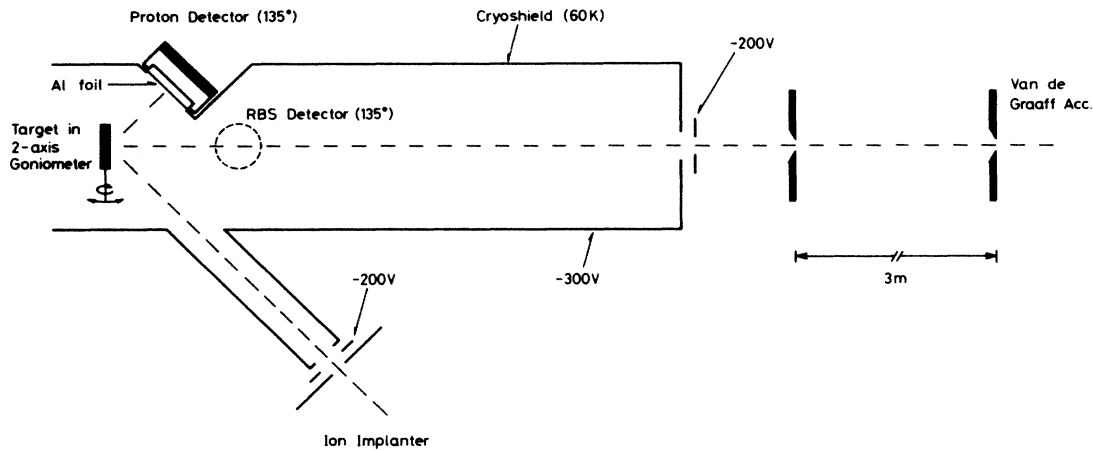


FIG. 2. Sketch of the experimental setup.

and the pressure was lower than $\sim 3 \times 10^{-7}$ torr. To avoid surface contamination of, e.g., hydrocarbons from the pumping oil, the target was surrounded by a cryoshield kept at a temperature of ~ 60 K by means of another cryogenic cooler.

The implantation was performed with a small ion accelerator equipped with an rf ion source, electrostatic deflection plates, and a magnet for isotope separation. The implantation beam was collimated to a circular spot of 7 mm diameter. The temperature during the implantation was kept at 30 K, and the implantation was performed with the beam direction 12° of the normal of the sample, i.e., far away from a major axis, to avoid channeling effects during the implantation. Deuterium ions were implanted at an energy of 10 keV, corresponding to a projected range of ~ 1500 Å. The current was $1 \mu\text{A}$ [$\sim 4 \times 10^{12}$ (D ions/cm²)/sec], and the total dose was, unless otherwise cited, 8×10^{14} D ions/cm², which give a local deuterium concentration of ~ 0.05 at. %.

The 750-keV ³He analyzing beam was supplied by a HVEC 2-MV Van de Graaff accelerator and was collimated by two slits 3 m apart, each set at 1×1 mm² (beam divergence $\leq 0.02^\circ$). The ³He ions backscattered from the silicon host were monitored in the Rutherford-backscattering-spectrometry (RBS) solid-state detector placed just below a window at the bottom of the cryoshield (Fig. 2). The implanted deuterium could be monitored with the aid of the "proton detector" (see Fig. 2), where the ~ 13 -MeV protons from the nuclear reaction $\text{D}({}^3\text{He}, p){}^4\text{He}$ were detected. In front of this detector was placed a 2- μm aluminum foil which allowed the protons to reach the detector while stopping the ~ 3.5 -keV α particles and the backscattered ³He ions. In this way, severe dead-time problems, caused by the large backscattering yield, were avoided. The cross section for the nuclear reaction was nearly constant to a depth of 0.7 μm , where it started to fall off, and the approximate probe depth was $\sim 1 \mu\text{m}$. The stopping power of the analyzing beam varied by a factor of ~ 2 in a scan through an axis, but this corresponded to only $\leq 2\%$ variations in the nuclear cross section in the implanted

region.

The implantation dose was determined from a comparison of the random proton yield with the yield of a Si-reference target implanted with 10^{16} D ions/cm² ($\pm 5\%$). The sensitivity of deuterium detection was rather high as ~ 2500 protons were detected when $1 \mu\text{C}$ of ³He was incident on 10^{16} D ions/cm².

The ion-beam current was measured to the target with the cryoshield biased to -300 V and, in one case, to the target and cryoshield in parallel. The results agreed to within $\pm 5\%$, indicating the absolute accuracy of the fluence. The cryoshield was electrically insulated from the cryocooler by mylar foil, while the target holder was insulated by a ceramic fitting.

The channeling analysis was carried out with simultaneous measurements of the proton and the backscattering yield, the latter being integrated over a depth interval corresponding to the range of the implanted deuterium. The fluence for each tilt angle was $3 \mu\text{C}$. To begin with, two linear orthogonal scans through the axis were performed over a range of $\sim \pm 0.4^\circ$ in steps of 0.1° to determine the position of the axis, which could be done with an accuracy of $\sim 0.03^\circ$. After this, full circular scans were performed for each new (increasing) tilt angle. Such a procedure has several advantages over the normal procedure with a linear scan through the axis. First, the initial distribution in transverse momentum space is very close to the equilibrium distribution, when a circular average is performed. Statistical equilibrium is therefore a better approximation, and the quantitative comparison of experimental scans with simulations based on the continuum model²⁹ with statistical equilibrium becomes more meaningful. Second, the reproducibility of the scans is improved, and, third, the measured random level, used to normalize all the data, is the right one according to the rule of angular compensation.²⁹ This is not true for linear scans, where planar effects often induce deviations of $\sim 10\%$ from the correct value.

The channeling analysis was always performed at 30 K around the $\langle 100 \rangle$, $\langle 110 \rangle$, and $\langle 111 \rangle$ axes and the $\{100\}$, $\{110\}$, and $\{111\}$ planes. Each new spot was irradiated

to a fluence of $10 \mu\text{C}$, with the analyzing beam aligned along the axis or plane before starting the channeling analysis. This was done to ensure that no changes in the deuterium signal occurred during the analysis (see Sec. III). The channeling scans were measured after the implantation and after isochronal annealing at various temperatures in the range 30–500 K. The annealing time was 10 min and, unless otherwise cited, the annealing preceded the $10\text{-}\mu\text{C}$ irradiation at 30 K. Finally, linear-ramp-annealing experiments were performed with the beam aligned along the $\langle 100 \rangle$ and the $\langle 110 \rangle$ axes.

III. BEAM-INDUCED ANNEALING AT 30 K

The analyzing beam induces changes in the channeling signals related to both the deuterium impurities and the host atoms. This is illustrated in Fig. 3, where the proton yield is shown together with the backscattering yield as a function of ^3He fluence when the analyzing beam is aligned with the $\langle 100 \rangle$ or the $\langle 110 \rangle$ axis. The measurements were performed at 30 K just after the implantation, and the yields have been normalized to the data points corresponding to the lowest fluence. When the analyzing beam is aligned with the $\langle 100 \rangle$ axis, both the proton and the backscattering yield decrease with increasing fluence. For the $\langle 110 \rangle$ axis, a fast decrease in the proton yield is followed by a slower increase, indicating that the effect involves two competing processes. However, the fast decrease at small fluences may be due

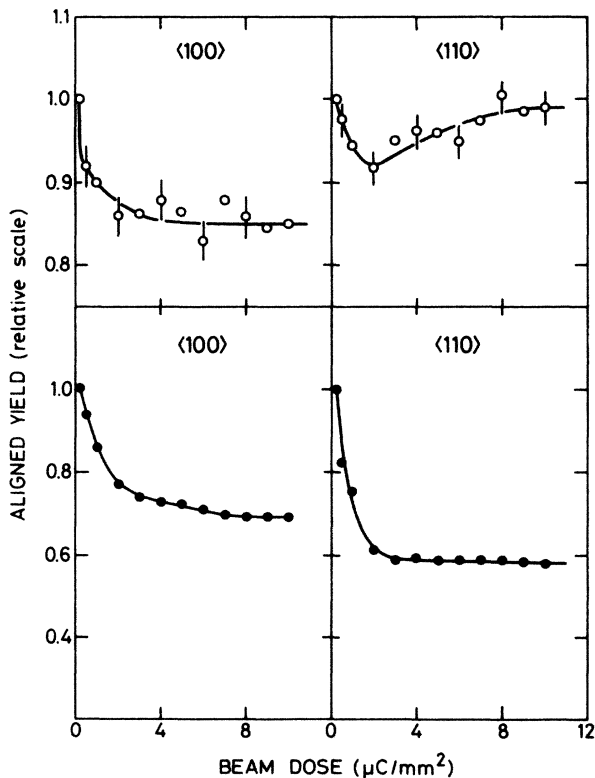


FIG. 3. The proton (\circ) and backscattering (\bullet) yields shown as functions of analyzing-beam fluence with the beam aligned with the $\langle 100 \rangle$ or the $\langle 110 \rangle$ axis.

to beam-induced desorption of deuterium atoms from the target surface, whereas the increase reflects a real change in the deuterium position during the bombardment. The measurements were extended to much higher fluences than shown in the figure, but no further changes in the aligned yield occurred after irradiation with $\sim 10 \mu\text{C}/\text{mm}^2$ ($\sim 6 \times 10^{15} \text{ } ^3\text{He}$ ions/ cm^2).

The decreases in the backscattering yields were also observed after implantation of 20-keV helium ions, showing that this beam effect is related to the annealing of intrinsic defects. Hence, it is possible to obtain direct information about these defects from measurements of curves similar to those presented in Fig. 3. Such measurements have been carried out, and the results were described in a recent paper,³⁰ to which the reader is referred for details. In the following, only a brief account of the main results of interest for the present work will be given.

A channeling analysis showed that 14% of all the silicon atoms in the damage region are displaced on the average by $\sim 0.25 \pm 0.10 \text{ \AA}$ from substitutional sites just after the implantation. In addition to this, there are 2% of the host atoms located interstitially with a displacement of approximately half a bond length (1.18 \AA) from a lattice site. The measurements are consistent with a displacement along a $\langle 110 \rangle$ or a $\langle 111 \rangle$ direction but not with a displacement along a $\langle 100 \rangle$ direction. In Ref. 30, the major near-substitutional component was ascribed to the relaxation of Si atoms around vacancy-type and interstitial-type defects, while the minor component was assigned to self-interstitials.

From considerations of the energies deposited by the analyzing beam into nuclear motion and ionization in the damage region, it was shown³⁰ that the beam annealing is

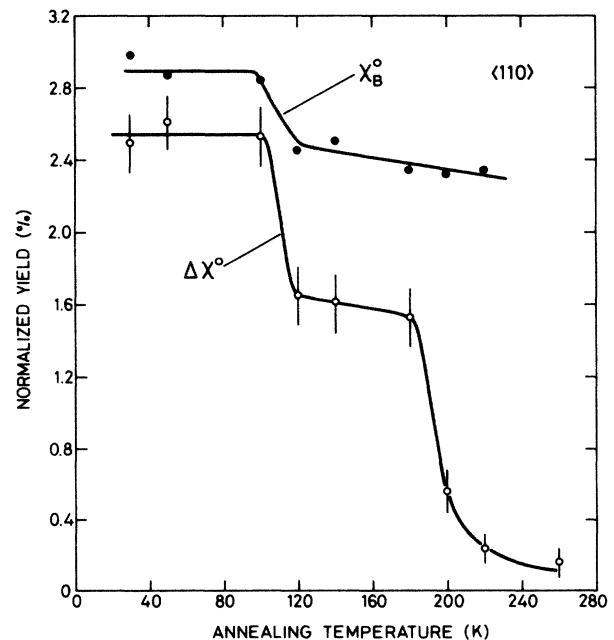


FIG. 4. The beam-induced signal $\Delta\chi^0$ as a function of isochronal annealing temperature (K). The background signal χ_B^0 is also shown.

due to the ionization by the analyzing beam. It was suggested that ionization-induced migration of both vacancies³¹ and self-interstitials³² is responsible for the observed effect.

It is possible to remove the damage, which disappears during beam annealing at 30 K, by a preceding thermal anneal, as illustrated in Fig. 4. The beam-induced signal $\Delta\chi^0$ is the part of the normalized aligned backscattering yield which disappears during the beam annealing, whereas χ_B^0 is the remaining (stable) part of the normalized yield. There is a stage with $\sim 35\%$ recovery at 110 K, which was ascribed to the migration of vacancies (probably V^-). A second annealing stage at ~ 190 K, leading to complete recovery, was assigned to the thermal migration of interstitials.

IV. CHANNELING SIMULATIONS

The lattice location of deuterium in the silicon lattice is determined from a comparison of the experimental channeling scans with the results of computer simulations corresponding to various deuterium sites. The details of the calculations will be published elsewhere,³³ and only a brief summary will be given here.

In order to calculate the angular dependence of the normalized yield related to a specific impurity site, one has to average over all the equivalent sites given by the symmetry of the lattice. Each equivalent site is projected onto the plane transverse to the axis (or the line transverse to the plane), and the averaging is performed over these positions in the transverse plane (or line), with each position being weighted according to its occurrence.

The calculations of this work are based on the continuum model,²⁹ and the thermal vibrations of both the impurity and the host atoms have been included. Two-dimensional vibrational amplitudes of 0.07 \AA (ρ_{Si}) for the host and 0.15 \AA (ρ_{D}) for deuterium have been applied, where ρ_{Si} is calculated with a Debye model,³⁴ and ρ_{D} is estimated from a typical vibrational frequency of hydrogen in silicon.

The simulations of axial scans are carried out with a thermally averaged multistring (~ 21 – 24 strings) Doyle-Turner potential³⁵ which can be written as

$$U_{\text{ax}}(\mathbf{r}) = \frac{8\pi^2 e^2 a_0 Z_1}{d} \sum_{\mathbf{R}} \sum_{i=1}^4 \frac{a_i}{b_i + (2\pi\rho_{\text{Si}})^2} \times \exp \left[-\frac{[2\pi(\mathbf{r}-\mathbf{R})]^2}{b_i + (2\pi\rho_{\text{Si}})^2} \right], \quad (1)$$

where e is the electron charge, a_0 the Bohr radius, Z_1 the Z value of the projectile, and d the distance between atoms along the string. The first summation is over all the strings, with positions $\{\mathbf{R}\}$, contributing to the potential at position \mathbf{r} , and the coefficients a_i and b_i are those given in Ref. 35.

With the assumption of statistical equilibrium on an energy shell in transverse phase space, the normalized yield χ for a given impurity site \mathbf{r}_{D} may be expressed as

$$\chi(\psi) = \int_0^\infty dE_\perp g(E_\perp, \psi, z) \Pi_{\text{in}}(E_\perp), \quad (2)$$

where ψ is the angle between the direction of the beam and the axis (tilt angle), $g(E_\perp, \psi, z)$ the distribution function for transverse energy E_\perp at depth z , and $\Pi_{\text{in}}(E_\perp)$ is the probability of a close-encounter process at the impurity site \mathbf{r}_{D} , normalized to the random value. If the area available inside one channel for particles with transverse energy E_\perp is denoted $A(E_\perp)$, and the total area of the channel is denoted A_0 , then the function $\Pi_{\text{in}}(E_\perp)$ can be calculated with the following formula:

$$\Pi_{\text{in}}(E_\perp) = \frac{A_0}{A(E_\perp)} \int_{U_{\text{ax}}(\mathbf{r}) \leq E_\perp} \exp[-(\mathbf{r}-\mathbf{r}_{\text{D}})^2/\rho_{\text{D}}^2] \frac{d\mathbf{r}}{\pi\rho_{\text{D}}^2}. \quad (3)$$

In the normal version of the continuum-model simulations, the energy distribution at zero depth [see Eq. (4)] has been inserted into Eq. (2). However, multiple scattering on nuclei and electrons leads to dechanneling, and the g function therefore depends on the depth. This can be taken into account with a diffusionlike equation,^{36,37} where the g function at depth z is found as the solution to the following system of equations:

$$g(E_\perp, \psi, z=0) = \frac{A'(E_\perp - E_0 \psi^2)}{A_0}, \quad (4)$$

$$\frac{\partial g}{\partial z}(E_\perp, \psi, z) = \frac{\partial}{\partial E_\perp} \left[A(E_\perp) D(E_\perp) \frac{\partial}{\partial E_\perp} \frac{g(E_\perp, \psi, z)}{A(E_\perp)} \right], \quad (5)$$

$$D(E_\perp) = \frac{1}{A(E_\perp)} \int_0^{E_\perp} A(\varepsilon) \frac{dE_\perp}{dz}(\varepsilon) d\varepsilon. \quad (6)$$

Here, E_0 is the beam energy, $D(E_\perp)$ the diffusion function,^{36,37} and dE_\perp/dz the increase in transverse energy per unit increase in penetration depth. We hope to give the analytical expression used to calculate the nuclear and electronic part of dE_\perp/dz in Ref. 33, together with a more comprehensive description of the program.

It is important to include dechanneling even though the implantation depth is only $\sim 1500 \text{ \AA}$. The main changes in the simulated substitutional host dip induced by dechanneling are a small increase in the minimum yield by ~ 0.005 and, in particular, a decrease in the width of the simulated dip by $\sim 10\%$. The experimental widths thereby become well reproduced by the simulations (see Fig. 7), and this agreement is found without adjusting any parameter (e.g., ρ_{Si}), indicating the quality of the present calculations. A discrepancy remains between the simulated and the measured minimum yield which is related to the well-known Barrett factor.³⁸ The substitutional site represents the least favorable case for the basic assumptions, and the correction factor becomes smaller for displaced sites.³⁸

In the case of the planar simulations, dechanneling has not been included, and as multiple-scattering effects are important for planar channeling, these simulations can only be used in qualitative analysis. The thermally averaged Doyle-Turner planar potential³⁵ is given by

$$U_p(x) = 4\pi^{3/2}e^2a_0Z_1N_p \times \sum_{x_p} \sum_{i=1}^4 \frac{a_i}{[b_i + (2\pi\rho_{Si})^2]^{1/2}} \times \exp\left[-\frac{[2\pi(x-x_p)]^2}{b_i + (2\pi\rho_{Si})^2}\right], \quad (7)$$

where N_p is the planar atomic density (atoms/cm²), x_p the position of one of the planes contributing to the potential, and ρ_{Si} is once again the two-dimensional vibrational amplitude of the host atoms. The normalized yield for a given site x_D may again be calculated from Eq. (2), where $\Pi_{in}(E_{\perp})$ and $g(E_{\perp}, \psi)$ now are given by

$$g(E_{\perp}, \psi, z=0) = \frac{L'(E_{\perp} - E_0\psi^2)}{L_0} \quad (8)$$

$$\Pi_{in}(E_{\perp}) = \frac{L_0}{\rho_D \sqrt{\pi}} \int_{U_p(x) \leq E_{\perp}} f_{E_{\perp}}(x) \times \exp[-(x-x_D)^2/\rho_D^2] dx, \quad (9)$$

$$f_{E_{\perp}}(x) = \frac{1}{[E_{\perp} - U_p(x)]^{1/2}} \times \left[\int_{U_p(x) \leq E_{\perp}} \frac{1}{[E_{\perp} - U_p(x)]^{1/2}} dx \right]^{-1}, \quad (10)$$

where L_0 is the distance between the atomic planes, and $L(E_{\perp})$ is the length of the allowed interval between two planes for particles with transverse energy E_{\perp} . These formulas are applicable for planes with equidistant spacing, whereas the equations become more complex for planes with alternating spacing³³ (e.g., {111} planes in silicon).

V. RESULTS

The conventional unit cell in the silicon lattice is shown in Fig. 1. As indicated in the figure, it is possible to divide the lattice into three different types of cubes, each of which has a unit length of one quarter of the lattice constant. All the cubes have equivalent *C* sites at six corners, and the differences between the cubes are given by the last two corners, where either two substitutional sites, one substitutional and one tetrahedral site, or two tetrahedral sites are located. In the interpretation of the channeling scans, it is therefore necessary only to focus the attention on the possible sites inside three small cubes, which facilitates the analysis of the data.

A. Results at 30 K

The experimental channeling scans obtained after the implantation and beam annealing at 30 K are shown in Fig. 5, together with the simulations corresponding to the sites illustrated in Fig. 1. From the $\langle 111 \rangle$ scan, it is seen that most of the deuterium atoms are located close to either the hexagonal (*H*), the antibonding (*Q*), or the bond-center site (BC), which all give the same angular

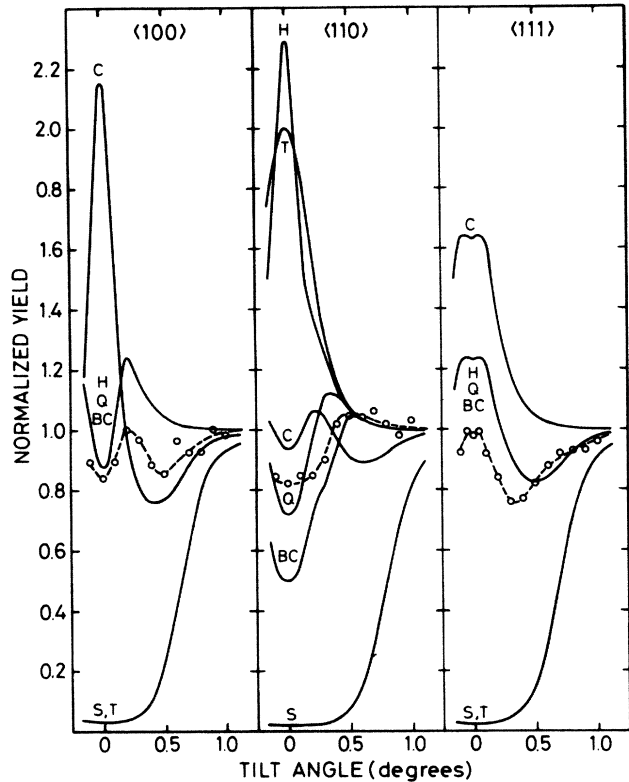


FIG. 5. The measured deuterium scans (\circ) after beam annealing at 30 K are shown for the three main axes together with the results of simulations corresponding to the sites shown in Fig. 1. The dashed lines through the data points are drawn to guide the eye.

scans through the $\langle 111 \rangle$ (and the $\langle 100 \rangle$) axis. The *H*, *Q*, and BC sites are very similar in the sense that they are located at the centers of rather similar cubes, and this explains why the channeling scans coincide for these two axes. The $\langle 110 \rangle$ axis is the only one of the major axes which gives rise to different scans for these three sites. From the figure, it is seen that the *H* site is inconsistent with the measured $\langle 110 \rangle$ scan as it should result in a strong flux peak, in contrast to the narrow dip observed. The width of the dip corresponds very well with the BC-site simulation, whereas the *Q*-site simulation seems a little too narrow, suggesting that the BC site is the right one. This is confirmed by the angular scan through the {111} plane shown in Fig. 6. As mentioned earlier, the planar simulations are expected only to reproduce the qualitative shape of the channeling curves, but as the *Q* and BC site should give rise to qualitatively very different angular scans through the {111} plane, it is possible to distinguish these two sites. Thus it is concluded that the *major* part of the deuterium atoms is located close to bond-center sites. This conclusion is also in agreement with the experimental $\langle 100 \rangle$ scan shown in Fig. 5, but at large tilt angles, 0.5°–1.0°, a weak dip component is observed. Such a behavior *cannot* be explained by a unique lattice location of deuterium at near-bond-center sites or anywhere else. The width of the dip indicates that the weak component is nearly shadowed by the $\langle 100 \rangle$ atomic

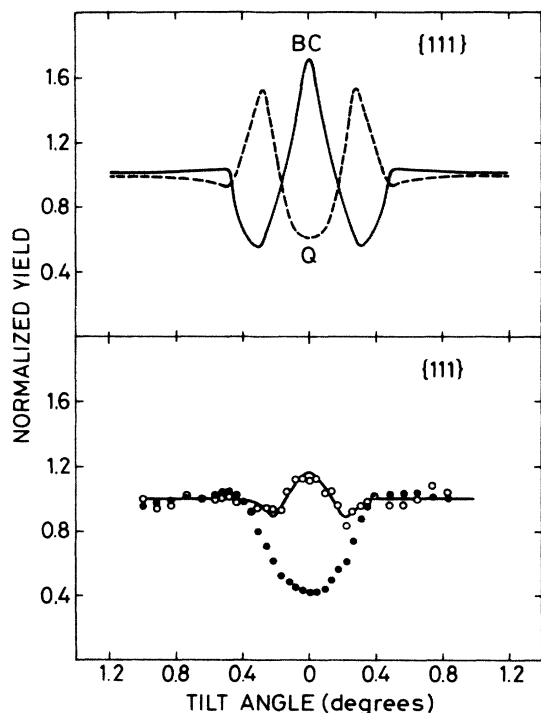


FIG. 6. The experimental $\{111\}$ -planar scan (lower part) shown together with the simulations (upper part), corresponding to the bond center (BC) and the antibonding sites (Q), respectively. The open symbols represent the deuterium data, whereas the solid symbols show the host scan.

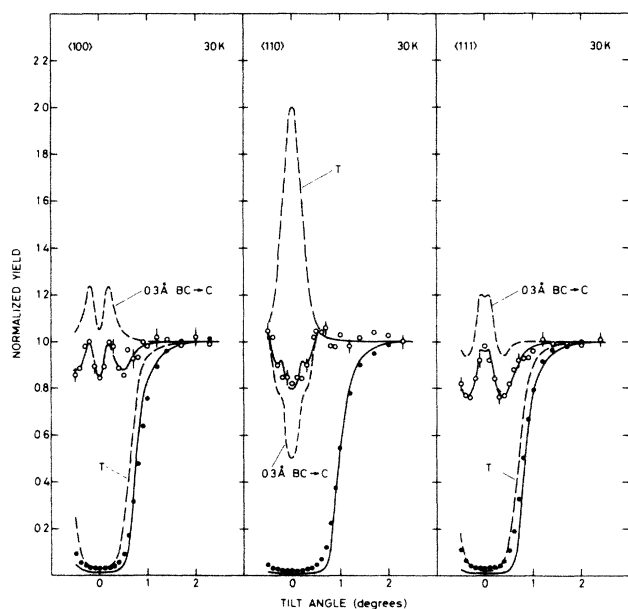


FIG. 7. Axial scans measured after beam annealing at 30 K shown together with the best fit to the deuterium scan (\circ). The fit (solid line) was obtained with 80% of the deuterium atoms displaced by 0.3 Å from bond centers towards C sites and the remaining 20% displaced by 0.1 Å from tetrahedral sites. Simulations corresponding to these two components are indicated by dashed lines. Finally, the Si-host scans (\bullet) are compared with the simulated host dips (solid lines).

strings. Both the substitutional sites (S) and the tetrahedral sites (T) are shadowed by all the $\langle 100 \rangle$ strings. However, the weak component cannot be located substitutionally as this should give rise to a dip at large tilt angles in the $\langle 110 \rangle$ scan, which is not observed. It can therefore be concluded that a *minor* part of the deuterium atoms is located close to tetrahedral sites.

Until now, the angular scans have been discussed from a qualitative point of view. A more detailed analysis has been performed to get the best possible fit to the data. The result is shown in Fig. 7, together with the experimental scans through all the major axes. These fits were obtained when $(80 \pm 3)\%$ of the deuterium atoms were displaced by 0.3 ± 0.1 Å from bond-center sites towards one of the nearby C sites, and the remaining $(20 \pm 3)\%$ were displaced by 0.1 ± 0.1 Å from tetrahedral sites. Unfortunately, the fits are insensitive to the direction of the displacement from the tetrahedral site, but as the displacement is very small, this does not give rise to large uncertainties in the position of the minor component. An excellent overall agreement between experiment and theory is observed. The reliability of these site identifications finds further support from the good qualitative agreement between the measured and the simulated planar scans, illustrated in Fig. 8. The uncertainties

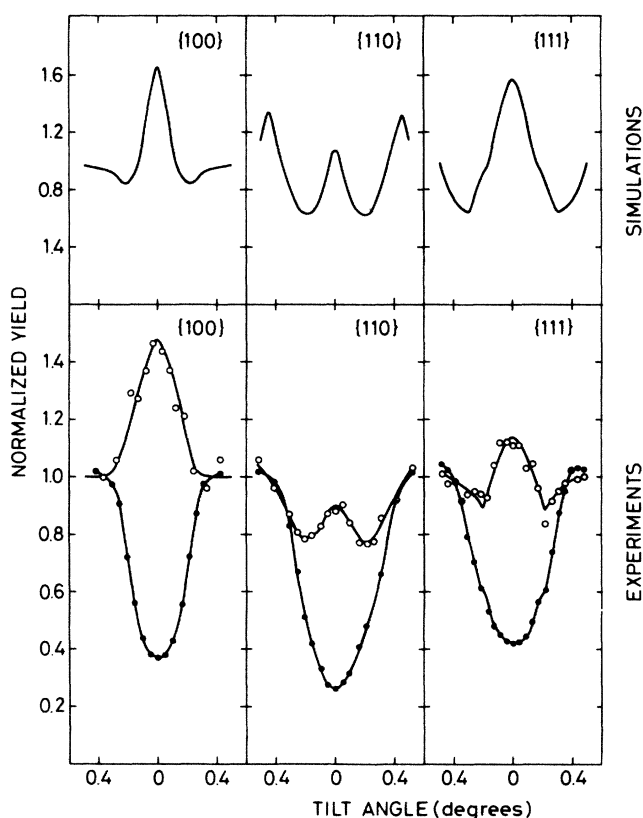


FIG. 8. Upper part: the simulated planar scans corresponding to 80% of the deuterium atoms displaced by 0.3 Å from bond centers towards C sites and the remaining 20% displaced by 0.1 Å from tetrahedral sites. Lower part: planar scans measured after beam annealing at 30 K. The deuterium scans are illustrated by open symbols (\circ), whereas the Si-host dips are shown by the solid symbols (\bullet). The solid lines through the data points are drawn to guide the eye.

given above were estimated from a visual comparison of the experimental data with the simulated curves calculated for various displacements and populations of the two sites.

B. Isochronal annealing experiments

The influence of a 10-min isochronal anneal at various temperatures on the $\langle 100 \rangle$ -aligned proton and backscattering yields is shown in Fig. 9. In this experiment, the beam spot was irradiated with $10 \mu\text{C}$ of ^3He before any thermal anneal was carried out. The aligned proton yield changes at ~ 140 K, where a decrease is observed, and at ~ 500 K, where the yield increases again. The Si-host signal starts to anneal around 200 K and continues to decrease at higher temperatures. There are indications of two annealing stages at ~ 200 –350 K and at ~ 400 –500 K. The latter stage corresponds to the increase in the deuterium yield at ~ 500 K, indicating that the same process is responsible for both changes.

In a linear-ramp annealing experiment (ramp rate 1 K/min), it was found that no deuterium atoms left the probe region during annealing up to 550 K. The stages at ~ 140 and ~ 500 K are therefore not related to long-

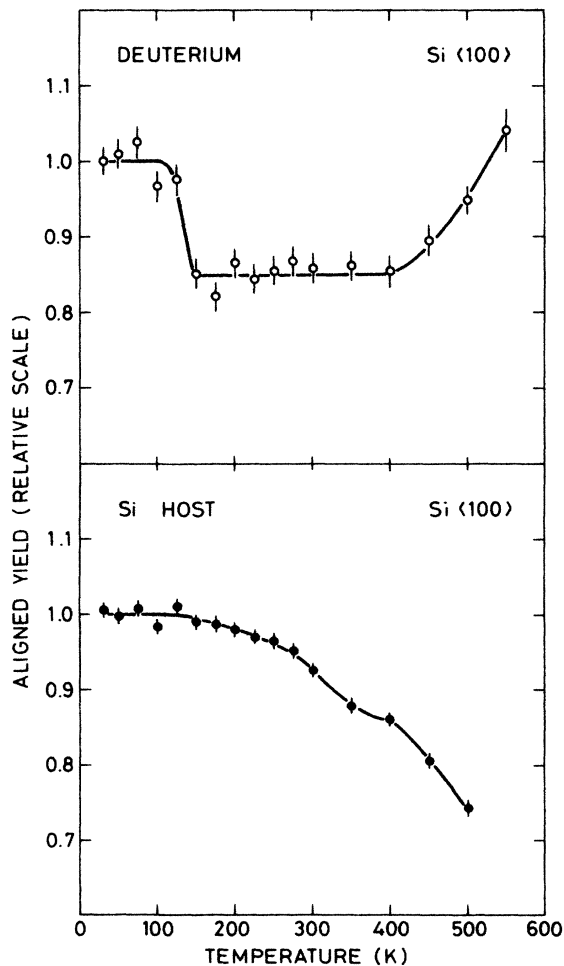


FIG. 9. The $\langle 100 \rangle$ -aligned yields shown as a function of isochronal-annealing temperatures. Beam annealing at 30 K preceded the thermal-annealing sequence.

range diffusion but involves changes of sites for, at least part of, the deuterium impurities. It is possible to get an idea of the changes that occur on the basis of Fig. 10, where the $\langle 100 \rangle$ scans obtained after annealing at various temperatures are shown. In these experiments, the thermal anneal preceded the irradiation at 30 K.

The first change in the $\langle 100 \rangle$ scan is observed between 125 and 150 K, corresponding to the 140-K stage. Qualitatively, the angular dependence is very much the same as that found at 30 K, suggesting that the major effect of a ~ 150 -K annealing is only to change the populations of the near-bond-center and the near-tetrahedral components relative to one another. From the figure, it is seen that the $\langle 100 \rangle$ -dip component increases and, according to the previous analysis, this corresponds to an increase of the population of the near-tetrahedral sites at the expense of the population of the near-bond-center sites (see Fig. 7).

With respect to the changes of sites after annealing at ~ 500 K, it is concluded that the major effect of this stage also is a redistribution of the deuterium atoms among the two components identified. In this case, the $\langle 100 \rangle$ -dip component is reduced substantially compared with the situation after annealing at 150 K, and the ~ 500 -K stage thus involves the growing of the near-bond-center component and the corresponding annealing of the near-tetrahedral component.

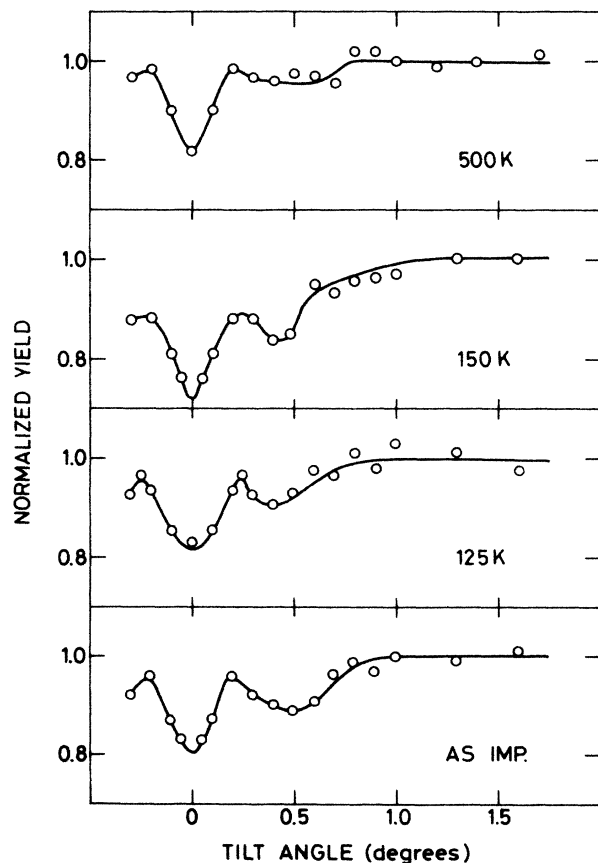


FIG. 10. $\langle 100 \rangle$ -axial deuterium scans measured after isochronal annealing at various temperatures. The thermal annealing preceded the beam annealing at 30 K.

These conclusions, based on a qualitative discussion of the $\langle 100 \rangle$ scans presented in Fig. 10, were confirmed by a detailed analysis analogous to that applied earlier. The population changes were obtained from the fits to the scans through the major axes, and again, excellent agreement between experiment and theory was observed, as illustrated in Fig. 11. After annealing at 150 K, $(30 \pm 3)\%$ of the deuterium atoms were located close to tetrahedral sites and the remaining $(70 \pm 3)\%$ close to bond centers. The positions giving the best fit were very close to those found at 30 K. The bond-center component was still displaced by $0.3 \pm 0.1 \text{ \AA}$ towards a C site, while the tetrahedral component was found to be displaced by $0.2 \pm 0.1 \text{ \AA}$ from the T site.

Further annealing at 200 and 300 K did not change the population of the two sites or the location of the tetrahedral component, but the best fit was now obtained with the major component being displaced by $0.3 \pm 0.1 \text{ \AA}$ from the BC site towards a nearby Y site. See Fig. 12, where the two near-bond-center sites are illustrated, together with the Y and C sites. The shift in position at 200 K is by no means large, and the corresponding differences observed in the angular scans are only slightly larger than what can be accounted for by statistical fluctuations.

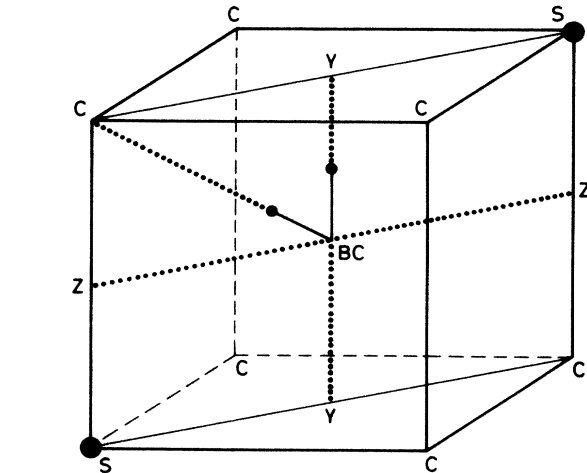


FIG. 12. The two identified near-bond-center sites are illustrated. The unit length of the cube is one quarter of the lattice constant, as seen in Fig. 1.

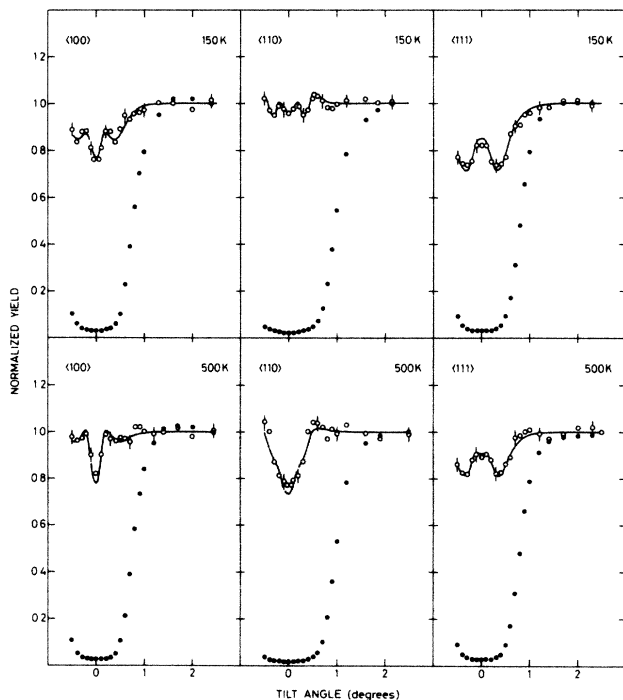


FIG. 11. Axial scans measured after annealing at 150 and 500 K. In all cases, the thermal annealing preceded irradiation at 30 K. The solid lines through the deuterium data points (\circ) show the best fit to the data. The fit to the 150-K data was obtained with 70% of the deuterium atoms displaced by 0.3 \AA from bond centers towards C sites, and the remaining 30% displaced by 0.2 \AA from tetrahedral towards hexagonal sites. The fit to the 500-K data was obtained with 85% of the deuterium atoms displaced by 0.3 \AA from bond centers towards Y sites (see Fig. 12) and 15% displaced by 0.2 \AA from tetrahedral sites towards hexagonal sites. Also the measured Si-host dips (\bullet) are shown.

tuations.

Finally, after annealing at 500 K, the fraction of deuterium atoms displaced by $0.2 \pm 0.1 \text{ \AA}$ from tetrahedral sites decreased to $(15 \pm 3)\%$, and the fraction displaced by $0.3 \pm 0.1 \text{ \AA}$ from bond centers towards Y sites increased to $(85 \pm 3)\%$.

C. Beam effects during linear-ramp annealing

It has already been described in Sec. III how the beam-induced annealing of implantation defects at 30 K gives rise to changes in the deuterium scans. This is not, however, the only effect of the analyzing beam observed in this work, as illustrated in Fig. 13. The figure shows how the aligned proton yield changed as a function of temperature during linear-ramp annealing when the beam was aligned with either the $\langle 100 \rangle$ or the $\langle 110 \rangle$ axis. The ramp rate was 1 K/min, and the beam effect at 30 K was removed with a preceding ^3He irradiation. The two stages at ~ 65 and ~ 90 K seen in the figure were not observed in the isochronal-annealing experiment (Fig. 9), demonstrating that the processes responsible cannot proceed without the presence of an analyzing beam at these temperatures. In an additional experiment, where the linear-ramp annealing was preceded by thermal annealing at 125 K, both stages at ~ 65 and ~ 90 K were observed again, confirming this conclusion.

The channeling scans did not change noticeably compared with the 30-K data when the analysis was preceded by an irradiation at 80 K, with the beam aligned with the axis. There was, however, an indication of a weak increase of the near-tetrahedral component, at the expense of the near-bond-center component. This is consistent with the decrease in the $\langle 100 \rangle$ -aligned proton yield and the corresponding weak increase in the case of the $\langle 110 \rangle$ direction observed at ~ 65 K (see Fig. 13). The changes in the populations of the two sites were found to be $\leq 3\%$, which is of the same order as the uncertainty.

The beam-induced change of sites at ~ 90 K had a

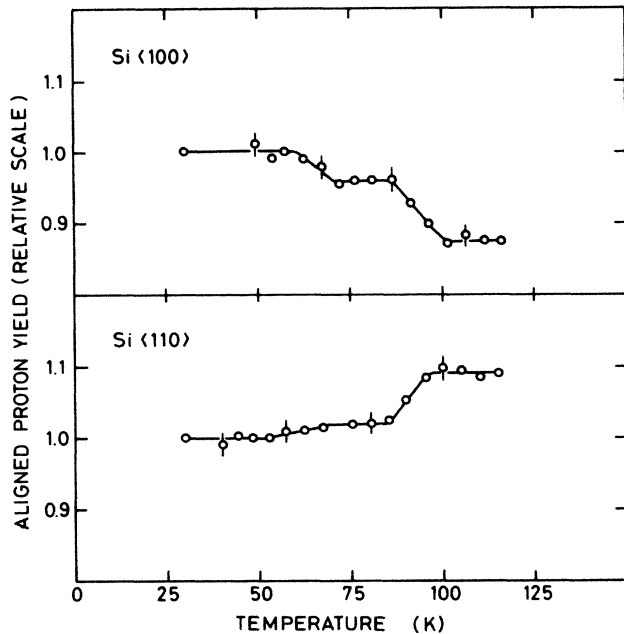


FIG. 13. The proton yields with the beam aligned with the $\langle 100 \rangle$ and the $\langle 110 \rangle$ axis are shown as a function of temperature during linear-ramp annealing. Irradiation at 30 K preceded the ramp annealing, and the ramp rate was 1 K/min.

larger effect on the channeling scans, as illustrated in Fig. 14. The angular scans presented in the figure were measured at 30 K after a preceding $30\text{-}\mu\text{C}$ irradiation at 30 K (\bullet) and 100 K (\circ), respectively, with the beam aligned with the axis. Also shown in the figure are the best fits to the data obtained from the present two-component analysis, with the near-bond-center component displaced by $0.3 \pm 0.1 \text{ \AA}$ towards the C site, and with the second component being displaced by $0.2 \pm 0.1 \text{ \AA}$ from the tetrahedral site. After $30\text{-}\mu\text{C}$ irradiation at 30 K, the fractions of atoms located at near-bond-center sites and near-tetrahedral sites were found to be $(78 \pm 3)\%$ and $(22 \pm 3)\%$, respectively, in agreement with the previous findings. These populations changed to $(62 \pm 3)\%$ for the near-bond-center component and to $(38 \pm 3)\%$ for the near-tetrahedral component when the irradiation was performed at 100 K.

Finally, in an additional experiment, the linear-ramp annealing was continued up to 270 K, and the only stages in the $\langle 100 \rangle$ -aligned proton yield were observed at ~ 65 and ~ 90 K, whereas the stage at ~ 140 K observed in the isochronal annealing experiment was absent.

VI. DISCUSSION

Some of the information obtained from the isochronal annealing experiments presented in this work and in Ref. 30 are sketched in Fig. 15 together with the results of infrared-absorption measurements.^{2,3} The infrared lines at 1840 and 2060 cm^{-1} were observed after implantation at low temperature³ (~ 80 K), but unfortunately, these samples were only annealed up to 300 K.³⁹ After room-temperature implantation, the same two lines² were ob-

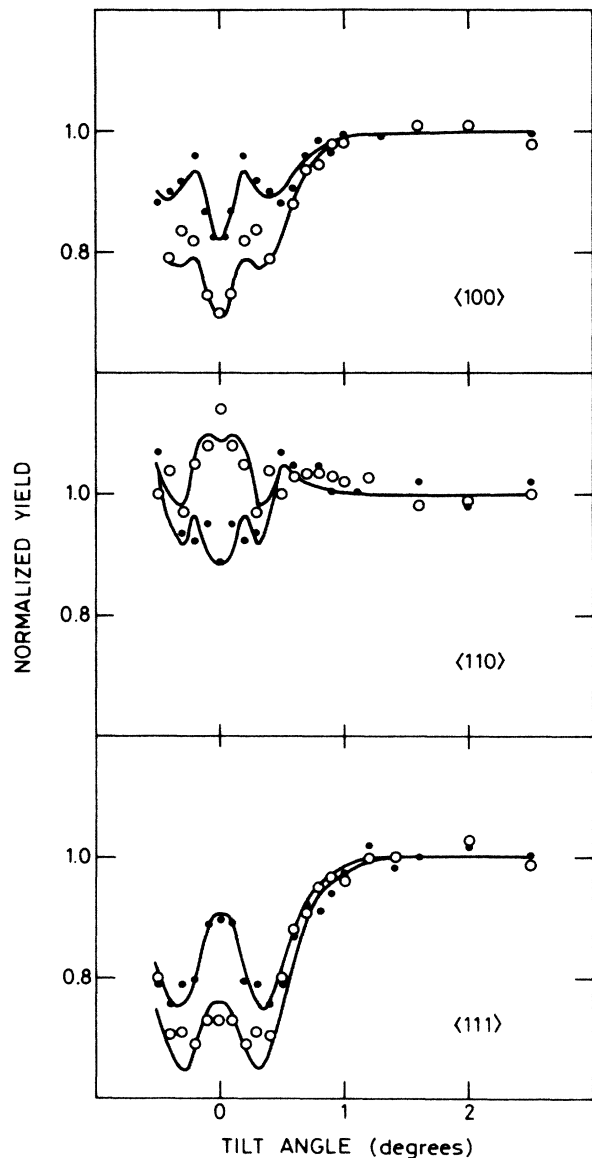


FIG. 14. Axial deuterium scans through the major axes measured after irradiation ($30 \mu\text{C}/\text{mm}^2$) at 30 K (\bullet) and 100 K (\circ). The solid lines represent fit to the data. After irradiation at 100 K (30 K), 62% (78%) of the deuterium atoms are displaced by 0.3 \AA from bond centers towards C sites, and the remaining 38% (22%) are displaced by 0.2 \AA from tetrahedral sites towards hexagonal sites.

served, and the annealing behavior has been sketched on the basis of these measurements at temperatures exceeding 300 K. The small shift of 5 cm^{-1} between the lines at 80 K and at room temperature is probably due to the difference in measuring temperature.

A. Interpretation of the deuterium sites

The implantation produces a large number of defects,^{30,40,41} and the spatial distribution of the damage peaks a little closer to the surface¹ than the depth profile of the implanted deuterium. The defect production is

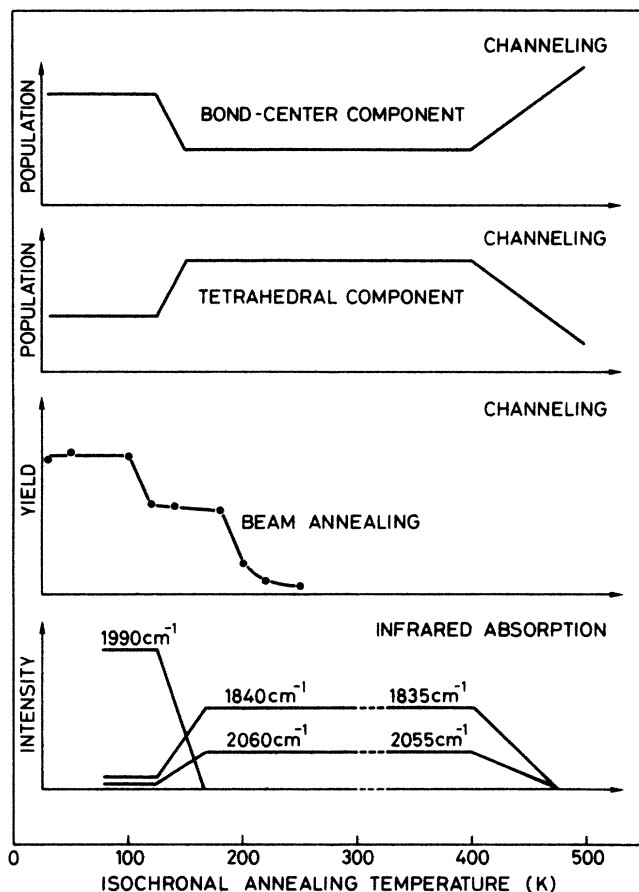


FIG. 15. The information on the changes of sites with temperature obtained in this work is sketched together with the annealing behavior of infrared-absorption lines and intrinsic defects (beam annealing). The information on infrared absorption is taken from Refs. 2 and 3.

correlated to the energy deposited in nuclear motion in the implanted region (see Table I). The number of Frenkel pairs created can be estimated from a modified Kinchin-Pease model, resulting in ~ 26 pairs per incoming deuterium ion. Thus the local deuterium concentration of 0.05 at % corresponds to a defect concentration of ~ 1.3 at %. In the analysis of the beam-induced annealing at 30 K, it was found that the concentration of interstitials (or split interstitials) was 2 at. % (or 1 at. %) (see Sec. III). The stable defects, which cannot be annealed by ^3He irradiation at 30 K, are not included in this estimate, but at low implantation doses ($\leq 10^{15}$ D ions/cm 2), the "unstable" defects dominate.³⁰ Therefore it is reasonable to assume that the defect concentration just

TABLE I. Energy deposited in the ~ 1500 -Å-thick implanted region during implantation and analysis.

Ion	Nuclear	Electronic
10-keV D $^+$	~ 1 keV	~ 9 keV
750-keV $^3\text{He}^+$	~ 70 eV	~ 47 keV

after the implantation is ~ 1 –2 at. %, as suggested by the Kinchin-Pease estimate.

The concentration of deuterium (~ 0.05 at. %), is several orders of magnitude larger than the concentration of impurities (e.g., donors, acceptors, oxygen, and carbon). Trapping at impurities can therefore be neglected in the interpretation of the identified sites. This has been confirmed experimentally as no differences were observed between measurements on *p*-type and *n*-type crystals of various resistivities and on float-zone and Czochralski-grown materials.

Later it is argued that there is more than one configuration associated with deuterium at near-bond-center sites. However, all the near-bond-center components are ascribed to deuterium atoms trapped at dangling bonds associated with vacancy-type defects, i.e., defects involving one or more vacancies. Several points can be made in favor of such an assignment. First, the position itself is a strong indication for trapping at vacancy-related dangling bonds. The distance from the deuterium site to one of the nearest substitutional sites is 1.3 ± 0.1 Å, in reasonable agreement with the bond length in silane (1.47 Å). If the distortions around vacancy-type defects (~ 0.25 Å) (Ref. 30) are taken into account, the agreement may be even better. Second, as discussed in the following subsection, the major near-bond-center component present below ~ 140 K BC(I), may be associated with the hydrogen-related infrared absorption line at 1990 cm $^{-1}$. This frequency is close to the stretch frequencies observed in silane²² and hydrogenated amorphous silicon,^{3,22} indicating the existence of strong covalent hydrogen-silicon bonds of the type found in these compounds. Third, according to the discussion above, there are plenty of vacancy-type defects present to account for the trapping. Finally, the results of theoretical calculations, based on MNDO calculations^{18,42} showed strong binding to vacancy-related dangling bonds.

It may be argued that when a deuterium atom is located close to the bond center, the presence of a vacancy-type defect has not been conclusively established in the discussion above. How can we exclude that the deuterium atoms break Si—Si bonds and then form the stronger Si—D bonds?¹² Such a mechanism has been suggested recently in order to explain the formation of anomalous muonium⁴³ in silicon. This would imply, however, that deuterium atoms in solution are located close to bond centers, in disagreement with theoretical calculations carried out for both the neutral^{42,44} and the positive¹⁹ charge state. Furthermore, due to nuclear repulsion, it is probably not possible for the deuterium atom to occupy a near-bond-center site without one of the two silicon atoms being displaced substantially from its lattice site. Hence the defect may be described as a deuterium-vacancy pair with a nearby interstitial, which is one of the possible configurations suggested in the following subsection.

In the discussion of the nature of the near-tetrahedral component, several possibilities have to be considered. These include deuterium atoms at solution sites, trapping at impurities, deuterium molecules located at tetrahedral sites and, finally, binding to interstitials. Some theoret-

cal calculations^{19,42} suggested that deuterium in solution is located at tetrahedral sites, but as the tetrahedral component is stable up to 400 K (see Fig. 15), and free migration sets in below room temperature (~ 170 K),¹⁷ this possibility is ruled out. Also trapping at impurities can be disregarded due to their low concentrations. The formation of molecules at the *T* site may be energetically favorable,^{18,19,44} as mentioned in the Introduction, but the deuterium atoms are displaced only by 0.2 ± 0.1 Å from tetrahedral sites, which would correspond to a molecular bond length of 0.4 ± 0.2 Å. This is much shorter than the bond length in vacuum¹² (0.74 Å), which probably even increases slightly⁴⁴ (by ~ 0.03 Å) when the molecule is introduced into the crystal. Furthermore, with concentrations of ~ 2 at. % vacancies and ~ 0.05 at. % deuterium atoms, the number of vacancy-related traps (dangling bonds) is 100–200 times the number of deuterium atoms, indicating that no substantial amount of molecules can be expected to form in these samples. Finally, from Fig. 15 it is seen that the annealing behavior of the near-tetrahedral component corresponds to that of the Si-H stretch frequencies observed at 1840 and 2060 cm^{-1} , indicating that the deuterium atoms at near-tetrahedral sites are associated with one of them and thus are chemically bound to silicon atoms. On the basis of this discussion the near-tetrahedral component is ascribed to binding of deuterium to an interstitial silicon atom. The interstitial may be a part of a larger defect containing both interstitials and vacancies, but we shall refer to this as trapping of deuterium at an interstitial-type defect.

A plausible defect structure accounting for such trapping is the self-interstitial which is believed to exist in two charge states I^{2+} and I^0 , according to calculations by Car *et al.*⁴⁵ and Bar-Yam and Joannopoulos.⁴⁶ The neutral self-interstitial was reported to have the exchange configuration,^{46,47} which is a $\langle 110 \rangle$ -split configuration, with the two silicon atoms located close to antibonding sites (*Q* sites). This location of the two interstitial Si atoms is consistent with our measurements on the defect structure,³⁰ summarized in Sec. III. An interesting point is that the calculations indicate⁴⁷ that the two interstitial atoms in the $\langle 110 \rangle$ -split configuration form bonds with the three nearest neighbors on lattice sites but not with one another, leading to dangling bonds pointing towards the open parts of the lattice in the neighborhood of tetrahedral sites. The distance from the *Q* site to the near-tetrahedral site is 1.4 Å, in good agreement with the bond length in silane¹² (1.47 Å). Furthermore, the distances to the three nearest lattice sites are 96% of a normal bond length in silicon, which seems to be a reasonable value for the Si—Si bond length associated with a defect. In the light of this discussion, a possible interpretation of the near-tetrahedral component is deuterium trapped at dangling bonds associated with neutral self-interstitials. However, it must be explained why the near-tetrahedral component anneals out at ~ 500 K, whereas the interstitials³⁰ disappear already at ~ 190 K (Fig. 14). The reason may be that the strong Si—D bond can retain the self-interstitial to much higher temperatures.

Thus, all the observed properties of both the near-tetrahedral component of deuterium and the interstitial silicon atoms can be accounted for consistently within this model. However, the specific assignment to trapping at neutral self-interstitials is only tentative.

For consistency, it has to be explained how all the deuterium atoms end up being trapped at 30 K. With a defect concentration at 2 at. %, the fraction trapped at defects just after the implantation is estimated to be only $\sim 9\%$, assuming a trapping radius equal to the Si—Si bond length (2.35 Å), and assuming that both deuterium atoms and defects are immobile. This value is much too low to account for the observations. The 100% trapping is, however, observed after ³He irradiation, which, as explained in Sec. III, induces changes in the location of the deuterium atoms. As mentioned earlier, the beam annealing has been ascribed to ionization-induced migration of vacancies and self-interstitials, and this is consistent with the observed trapping of deuterium atoms at dangling bonds related to these defects. The defects simply may migrate around until they either combine with a deuterium atom and form a stable center, or annihilate at other defects.

B. Interpretation of annealing stages

In the previous subsection, it was argued that the deuterium atoms may be trapped during the beam-induced migration of vacancies and interstitials. The thermally induced migration of vacancies and interstitials sets in at ~ 110 and ~ 190 K, respectively, according to our previous findings³⁰ (see Sec. III). We may therefore at a first sight expect the channeling scans to change after annealing at these temperatures, in contrast to our observations. This does not, however, represent an inconsistency. The channeling analysis is always preceded by the irradiation at 30 K, and therefore all the vacancies and interstitials disappear before any measurement is carried out, and the absence of stages at 110 and 190 K may be expected.

The decrease in the population of the near-bond-center sites and the related increase in the near-tetrahedral component after annealing at ~ 140 K was observed whether the irradiation at 30 K was carried out before or after the thermal annealing. The site changes at 140 K are therefore not related to defects that disappear during beam annealing. Furthermore, as seen in Fig. 9, the aligned Si-backscattering yield did not change at this temperature, indicating that no annealing of the intrinsic defects surviving the beam annealing is involved. This suggests that the stage is due to either migration of deuterium or annealing of deuterium-related defects. Deuterium is not expected to become mobile before ~ 170 K, as seen from extrapolation of high-temperature diffusion data.¹⁷ In addition, when the beam annealing is preceded by thermal annealing, the deuterium atoms are trapped already at 30 K according to the previous discussion, and free-deuterium migration at 140 K is therefore ruled out. Thus the change of site at 140 K is ascribed to the annealing of a deuterium-related defect. Now the drop in the population of near-bond-center sites after annealing at ~ 140 K corresponds very well to the annealing of the

hydrogen-related absorption line at 1990 cm^{-1} (see Fig. 15). Moreover, this is the dominating line in the infrared absorption spectra below 140 K just as the near-bond-center component is the dominating one observed in the channeling measurements. It is therefore suggested that the 1990-cm^{-1} line is associated with a near-bond-center component, denoted BC(I), which disappears after annealing at $\sim 140\text{ K}$. Even though the BC(I) complexes anneal out at $\sim 140\text{ K}$, a strong near-bond-center component is still present at higher temperatures (see Fig. 15). Thus it is concluded that a second near-bond-center component BC(II) exists which is stable at temperatures above 140 K.

A positive identification of the mechanism behind the annealing of BC(I) at 140 K is not possible on the basis of this work alone, but nevertheless some remarks can be made. At least a part of the deuterium atoms associated with BC(I) are transferred to near-tetrahedral sites at $\sim 140\text{ K}$. It is probably necessary to break the Si—D bond in order to do so, but the temperature seems much too low to thermally dissociate the very strong Si—D bond.¹² Tentatively, the annealing process is therefore ascribed to an additional silicon atom jumping into the central vacancy binding the deuterium atom, whereby a new Si—Si bond may be formed, while the deuterium atom is kicked out of the near-bond-center site. It seems plausible that the additional silicon atom comes from a nearby interstitial site, and that the annealing proceeds by a close-pair-recombination process. Such an assignment of the 140-K stage is also qualitatively consistent with a migration of free interstitials³⁰ at the somewhat higher temperature of $\sim 190\text{ K}$.

The annealing of the tetrahedral component around 500 K proceeds parallel with a decrease in the aligned backscattering yield from the silicon host, as illustrated in Fig. 9. This stage may therefore be associated with migration of intrinsic defects. The annealing temperature corresponds very well with that reported for migration of planar tetravacancies,⁴⁸ indicating that this defect could be responsible for the observed stage. Another possibility could be migration of divacancies,⁴⁹ but the annealing temperature seems a little too low. It is possible that interstitials binding the deuterium atoms annihilate with the migrating tetravacancies or divacancies, leaving free deuterium atoms, which are mobile at this temperature and therefore may be trapped at dangling bonds surrounding vacancy-type defects, in accordance with the observations.

From Fig. 15 it is seen that the infrared-absorption lines at 1840 and 2060 cm^{-1} have the same annealing behavior as the tetrahedral component. This suggests that at least one of them is associated with deuterium atoms at near-tetrahedral sites. According to the previous discussion, however, both the BC(II) component and the near-tetrahedral components are associated with Si—D bonds and both complexes are therefore expected to be infrared active. In the light of this, it is tentatively suggested that one of the lines at 1840 and 2060 cm^{-1} is associated with the near-tetrahedral component and the other with the BC(II) component. As seen from Fig. 15 this assignment implies that both the BC(II) and the near-tetrahedral components increase in strength at 140 K, where the

BC(I) component anneals out. The reason that the absorption line related to the BC(II) component also anneals out at $\sim 500\text{ K}$ is probably that the relevant vacancy-type defect trapping the deuterium atom becomes more complex due to clustering. This is consistent with the observation that new hydrogen-related absorption lines at 1931 and 2030 cm^{-1} grow up when the lines at 1835 cm^{-1} (1840 cm^{-1}) and 2055 cm^{-1} (2060 cm^{-1}) anneal out.²

C. Beam-induced effects

The influence of the beam-induced annealing at 30 K on the channeling scans has already been discussed and only the stages observed at ~ 65 and $\sim 90\text{ K}$ in the linear-ramp-annealing experiments will be dealt with here.

The vacancy in the doubly negative charge state has been reported to migrate at $\sim 60\text{--}80\text{ K}$ in silicon,⁵⁰ indicating that this defect may be responsible for the 65-K stage. However, the linear-ramp-annealing experiment shown in Fig. 13 was preceded by irradiation at 30 K, and thus neither vacancies or interstitials should be present at 65 K. This is seemingly in conflict with an assignment of the weak 65-K stage to vacancy migration, but as the analyzing beam also creates Frenkel pairs in the implantation region (~ 2 pairs/ion in a random direction), it may still be that vacancies are responsible for this stage.

Qualitatively, the irradiation at $\sim 90\text{ K}$ induced the same changes in the channeling scans as thermal annealing at $\sim 140\text{ K}$ and, moreover, the 140-K stage was not observed in the linear-ramp-annealing experiment. From this, it is concluded that the beam-induced stage at 90 K involves the same process, giving rise to the thermally activated stage at 140 K. This is also consistent with the infrared-absorption data,³ where annealing of the 1990-cm^{-1} line was observed after long-time illumination with light at $\sim 80\text{ K}$.

The near-tetrahedral component increased from 20% to 38% during irradiation at $\sim 90\text{ K}$, whereas thermal annealing at 140 K preceded by irradiation at 30 K increased this component only to 33%. This indicates that the process is more effective when it is induced by irradiation at 90 K than when it is induced thermally at 140 K. The difference between the increases (5%) is, however, only slightly larger than the uncertainty ($\pm 3\%$). A possible explanation of the difference is that the defects created by the analyzing beam are playing an active role in the increase of the near-tetrahedral component during the irradiation at 90 K. As discussed above, indications for this are observed already during irradiation at $\sim 65\text{ K}$.

D. Comparison with other experiments

It is natural to compare these results with those obtained by Picraux and Vook¹ even though the implantation and the measurements were performed at room temperature in their work. As previously mentioned, the only thermally induced annealing stage between 30 K and room temperature can be induced by irradiation at $\sim 90\text{ K}$. Furthermore, as no beam effects have been observed

above this temperature, the influence of the beam on the channeling scans may be similar at 100 K and at room temperature. As a consequence it is reasonable to compare the scans of Picraux and Vook (Figs. 2, 4, and 6 in Ref. 1)⁵¹ with those shown in Fig. 14, obtained after irradiation at 100 K. It is found that the two measurements are qualitatively and, within reasonable limits, quantitatively consistent.

Picraux and Vook¹ interpreted their results in terms of a single site displaced by 1.6 Å from a substitutional site in the antibonding direction. Such a site cannot account for the scans obtained in this work, whereas a satisfactory agreement is obtained between experiments and simulation with the two components identified here. Thus it is argued that the conclusion of Picraux and Vook is wrong.

The present work may also be compared with the results of the pion^{24,25} and muon^{26,27} blocking experiments. It must be emphasized, however, that the defect concentration is believed to be very small in those experiments, and a direct comparison may therefore be dubious. In spite of this, it is interesting to note that anomalous muonium in silicon has a spin Hamiltonian with $\langle 111 \rangle$ axial symmetry,⁵² anneals out at ~ 150 K,⁵³ and that recent blocking experiments are consistent with a near-bond-center site.⁴³ All these properties are consistent with the BC(I) configuration discussed herein.

VII. SUMMARY

These measurements have given information on the structure of deuterium-related defects in silicon in the temperature range 30–500 K. Intrinsic defects are found to be mobile during the ³He irradiation at 30 K preceding the channeling analysis, and only defect-related sites are observed in the detailed scans. The analysis shows that (80±3)% of the deuterium atoms occupy near-bond-center sites at 30 K, while the remaining (20±3)% are located at near-tetrahedral sites.

The measurements together with infrared absorption data have revealed that there are different configurations

corresponding to deuterium located at near-bond-center sites. The dominating near-bond-center configuration at low temperatures BC(I) is interpreted as a deuterium atom passivating a dangling bond associated with a vacancy-type defect in the presence of a nearby interstitial. Furthermore, this configuration has been associated with the 1990-cm⁻¹ absorption line observed earlier³ after hydrogen implantation into silicon. At ~ 140 K, this center anneals out, and it is suggested that the annealing may proceed by a close-pair-recombination process.

A second near-bond-center component BC(II) is also ascribed to a deuterium atom saturating a dangling bond associated with a vacancy-type defect. This component is stable up to ~ 500 K, where tetravacancies and/or divacancies start to migrate, and the defect becomes more complex probably due to the clustering of vacancies.

The near-tetrahedral component is assigned to deuterium trapped at an interstitial-type defect, and it anneals out at ~ 500 K, probably due to annihilation of the deuterium-related interstitials with migrating tetravacancies or divacancies.

The changes in the scans observed after annealing at 140 K can be activated at ~ 90 K during irradiation with the analyzing beam. Another beam-induced stage at ~ 65 K induced only very small changes in the angular scans, possibly due to migration of vacancies created by the analyzing beam.

The results of this work are consistent with the earlier infrared-absorption studies.³ The combination of the two techniques is powerful, as it allows us to relate information on lattice location to the bonding properties, and thus it can be very helpful in understanding the structure of hydrogen-related defects.

ACKNOWLEDGMENT

Numerous simulating discussions with J. U. Andersen concerning the interpretation of the data are gratefully acknowledged.

¹S. T. Picraux and F. L. Vook, *Phys. Rev. B* **18**, 2066 (1978).

²H. J. Stein, *J. Electron Mater.* **4**, 159 (1975).

³H. J. Stein, *Phys. Rev. Lett.* **43**, 1030 (1979).

⁴T. S. Shi, S. N. Sahu, G. S. Oehrlein, and J. W. Corbett, *Phys. Status Solidi A* **74**, 329 (1982).

⁵B. N. Mukashev, K. H. Nussopov, M. F. Tamendarov, and V. V. Frolov, *Phys. Lett.* **87A**, 376 (1982).

⁶C. Dubé and J. I. Hanoka, *Appl. Phys. Lett.* **45**, 1135 (1984).

⁷V. V. Kveder, R. Labusch, and Y. A. Ossipyan, *Phys. Status Solidi A* **84**, 149 (1984).

⁸J. L. Benton, C. J. Doherty, S. D. Ferris, D. L. Flamm, L. C. Kimerling, and H. J. Leamy, *Appl. Phys. Lett.* **36**, 670 (1980).

⁹C. H. Seager and D. S. Ginley, *J. Appl. Phys.* **52**, 1050 (1981).

¹⁰N. M. Johnson, D. K. Biegelsen, and M. D. Moyer, *Appl. Phys. Lett.* **40**, 882 (1982).

¹¹J. I. Pankove, M. A. Lampert, and M. L. Tarng, *Appl. Phys. Lett.* **32**, 439 (1978).

¹²T. L. Cottrell, *The Strength of Chemical Bonds* (Butterworths, London, 1954), p. 273.

¹³R. L. Kleinhenz, Y. H. Lee, V. A. Singh, P. M. Mooney, A.

Jaworoski, L. M. Roth, J. C. Corelli, and J. W. Corbett, in *Defects and Radiation Effects in Semiconductors, 1978*, Inst. Phys. Conf. Ser. No. 46, edited by J. H. Albany (IOP, London, 1978), p. 200.

¹⁴W. E. Spear and P. G. Le Comber, *Solid State Commun.* **17**, 1193 (1975).

¹⁵H. Fritzsche, C. C. Tsai, and P. Persans, *Solid State Technol.* **21**, 55 (1978).

¹⁶S. J. Pearton and A. J. Tavendale, *Phys. Rev. B* **26**, 7105 (1982).

¹⁷A. V. Vieringen and N. Warmoltz, *Physica* **22**, 849 (1956).

¹⁸J. W. Corbett, S. N. Sahu, T. S. Shi, and L. C. Synder, *Phys. Lett.* **93A**, 303 (1983).

¹⁹A. Mainwood and A. M. Stoneham, *J. Phys. C* **17**, 2513 (1984).

²⁰J. L. Nørskov, *Phys. Rev. B* **20**, 446 (1979).

²¹T. S. Shi, L. M. Xie, G. R. Bai, and M. W. Qi, *Phys. Status Solidi B* **131**, 511 (1985).

²²M. Cardona, *Phys. Status Solidi B* **118**, 463 (1983).

²³K. L. Brower (private communication).

- ²⁴W. Sigle, H.-D. Carstanjen, G. Flik, D. Herlach, G. Jünemann, K. Maier, H. Rempp, A. Seeger, R. Abela, D. Anderson, and P. Glasow, *Nucl. Instrum. Methods B* **2**, 1 (1984).
- ²⁵K. Maier, *Hyperfine Interact.* **17-19**, 3 (1984).
- ²⁶B. D. Patterson, A. Bosshard, U. Straumann, P. Truöl, A. Wüest, and T. Wichert, *Hyperfine Interact.* **17-19**, 965 (1984).
- ²⁷B. D. Patterson, *Hyperfine Interact.* **17-19**, 517 (1984).
- ²⁸B. Bech Nielsen, in *Oxygen, Carbon, Hydrogen, and Nitrogen in Crystalline Silicon* (Eds. J. C. Mikkelsen, S. J. Pearton, J. W. Corbett, and S. J. Pennycook, Vol. 50 of *MRS Symposia Proceedings* (Materials Research Society, Pittsburgh, 1986), p. 487).
- ²⁹J. Lindhard, K. Dan. Vidensk. Selsk. Mat. Fys. Medd. **34**, 14 (1965).
- ³⁰B. Bech Nielsen and J. U. Andersen, *Phys. Rev. B* **35**, 2732 (1987).
- ³¹G. D. Watkins, J. R. Troxell, and A. P. Chatterjee, in *Defects and Radiation Effects in Semiconductors, 1978*, Ref. 13, p. 16.
- ³²G. D. Watkins, in *Radiation Damage in Semiconductors* (Dunod, Paris, 1965), p. 97.
- ³³B. Bech Nielsen and J. U. Andersen (unpublished).
- ³⁴D. S. Gemmel, *Rev. Mod. Phys.* **46**, 129 (1974).
- ³⁵P. A. Doyle and P. S. Turner, *Acta Crystallogr. Sect. A* **24**, 390 (1968).
- ³⁶E. Bonderup, H. Esbensen, J. U. Andersen, and H. E. Schiøtt, *Radiat. Eff.* **12**, 261 (1972).
- ³⁷H. E. Schiøtt, E. Bonderup, J. U. Andersen, and H. Esbensen, in *Atomic Collisions in Solids*, Gatlinburg Conference, edited by S. Datz *et al.* (Plenum, New York, 1975), Vol. 2, p. 843.
- ³⁸J. H. Barrett, F. Fujimoto, K. Komako, and Y. Hashimoto, *Radiat. Eff.* **28**, 119 (1976).
- ³⁹H. J. Stein (private communication).
- ⁴⁰L. C. Kimerling, P. Blood, and W. M. Gibson, in *Defects and Radiation Effects in Semiconductors, 1978*, Ref. 13, p. 273.
- ⁴¹D. A. Thompson and R. S. Walker, *Radiat. Eff.* **30**, 37 (1976).
- ⁴²V. A. Singh, C. Weigel, J. W. Corbett, and L. M. Roth, *Phys. Status Solidi B* **81**, 637 (1977).
- ⁴³B. D. Patterson (private communication).
- ⁴⁴T. S. Shi, S. N. Sahu, J. W. Corbett, and L. C. Snyder, *Sci. Sin. A* **27**, 98 (1984).
- ⁴⁵R. Car, P. J. Kelly, A. Oshiyama, and S. Pantelides, in *Proceedings of the 17th International Conference on the Physics of Semiconductors, San Francisco, 1984*, edited by J. D. Chadi and W. A. Harrison (Springer-Verlag, New York, 1985), p. 711.
- ⁴⁶Y. Bar-Yam and J. D. Joannopoulos, in *Proceedings of the 17th International Conference on the Physics of Semiconductors, San Francisco, 1984*, Ref. 45, p. 721.
- ⁴⁷V. A. Telezhkin, *Fiz. Tekh. Poluprovodn.* **19**, 2023 (1985) [*Sov. Phys.—Semicond.* **19**, 1245 (1985)].
- ⁴⁸W. Jung and G. S. Newell, *Phys. Rev.* **132**, 648 (1963); K. L. Brower, *Radiat. Eff.* **8**, 213 (1971).
- ⁴⁹L. J. Cheng, J. C. Corelli, J. W. Corbett, and G. D. Watkins, *Phys. Rev.* **152**, 761 (1966).
- ⁵⁰G. D. Watkins, in *Lattice Defects in Semiconductors*, Inst. Phys. Conf. Ser. No. 23, edited by H. A. Huntley (IOP, London, 1975), p. 1.
- ⁵¹In Ref. 1 two $\langle 111 \rangle$ scans (Figs. 2 and 5) are presented. A close inspection of Fig. 5 reveals that the host scan is asymmetric, probably as a consequence of planar effects, and therefore, the scan in Fig. 2 has been compared with the result of the present work.
- ⁵²B. D. Patterson, A. Hinterman, W. Kündig, P. F. Meier, F. Waldner, H. Graf, E. Recknagel, A. Weidinger, and Th. Wickert, *Phys. Rev. Lett.* **40**, 1347 (1978).
- ⁵³B. D. Patterson, in *Muons and Pions in Materials Research*, edited by J. Chappert and R. I. Grynspan (Elsevier, New York, 1984), p. 161.